PNAS

Supporting Information for

Somatostatin Regulates Central Clock Function and Circadian Responses to Light

Deborah A.M. Joye, Kayla E. Rohr, Kimberlee Suenkens, Alissa Wuorinen, Thomas Inda, Madeline Arzbecker, Emma Mueller, Alec Huber, Harshida Pancholi, Murray G. Blackmore, Vania Carmona-Alcocer, Jennifer A. Evans

Marquette University, Department of Biomedical Sciences

Corresponding author:
Jennifer Evans
560 N 16th St,
Schroeder Complex, Room 446
Milwaukee, WI 53233
Phone: 414 288-5732
Fax: 414-288-6564
Email: jennifer.evans@marquette.edu

This PDF file includes:

Supplementary Methods

Mice and husbandry conditions

Mice were bred and raised under a 24-hour light-dark cycle with 12 hours of light and 12 hours of darkness [L12; lights off: 1800 CST defined as Zeitgeber Time 12 (ZT12)]. Throughout life, ambient temperature was maintained at 22°C ± 2°C, and mice had *ad libitum* access to water and food (Teklad Rodent Diet 8604). At weaning, mice were group housed in cages without running wheels. For experiments, mice were transferred to individual wheel-running cages. During experiments, mice remained relatively undisturbed except for routine husbandry. Cages were changed once every 2-3 weeks starting 30-60 min before ZT12 under entrained conditions. Under constant conditions, the time of activity onset was projected using linear regression fits and cage changes were executed under dim red light in the hour before onset to minimize disturbance in activity record. Both male and female mice were used in all experiments unless otherwise noted. All procedures were conducted according to the NIH Guide for the Care and Use of Animals and were approved by the Institutional Animal Care and Use Committees at Marquette University.

Genetic labeling of SCN neurons

To genetically label *Sst* neurons, Sst-IRES-Cre mice (1), JAX#018973, C57Bl/6N background) were crossed to Ai9 mice (2). In progeny of this cross, Cre recombinase is expressed under the *Sst* promoter, causing cell-specific expression of the red fluorescent protein, tdTomato. This genetic approach permanently labels cells after *Sst* transcription regardless of continued expression or daily variation in peptide transcript expression, thus circumventing the need for a circadian time course. To compare the SCN *Sst*-tdT+ cells to those of other SCN peptide groups, Ai9 mice were also crossed to Vip-IRES-Cre mice (1), JAX# 010908, C57Bl/Jx129S background) and Avp-IRES-Cre mice (3), JAX# 023530, C57Bl/6 background). For spatial mapping of cellular subpopulations, *Sst*-, *Vip*- and *Avp*-IRES-Cre$^{+/-}$;Ai9$^{+/-}$ mice were maintained on a L12 photoperiod under colony conditions, and brains were collected in the middle of the day (i.e., ZT06). To test light-activated changes in *Sst*-tdT+ expression, *Sst*-IRES-Cre$^{+/-}$;Ai9$^{+/-}$ mice (10-21 weeks starting age) were entrained to L12 or L20 in behavioral chambers for 1-12 weeks (n = 7-14/group/entrainment duration). Brains were collected in the middle of the day (i.e., ZT06). Because tdT is a permanent label (3), we predicted that the number of *Sst*-tdT+ labelled cells would increase in L20 if long day entrainment induces *de novo* activation of *Sst* transcription.

Immunohistochemistry (IHC)

Sst-tdT labelling was complemented with SST immunohistochemistry (IHC). *Sst*-IRES-Cre$^{+/-}$;Ai9$^{+/-}$ mice (13 weeks of age, n = 5-11/sex) were maintained on L12. Brains were collected at ZT00, ZT06, ZT12, or ZT18 (n = 4/timepoint) under bright white light or dim red light conditions dependent on ZT. To test photoperiodic changes in overall SST expression, male and female PER2::LUC$^{+/+}$ mice (13 weeks of age, n = 12/sex) were exposed to a photocycle with either 12 h, 18 h, or 6 h of light per day (L12, L18, L06, n = 8/photoperiod) before receiving 1µl colchicine injection into the third ventricle (0.5µl/min) to slow microtubule transport and measure cumulative SCN SST expression over the circadian cycle. To test that lack of SST alters SCN neurochemistry, *Sst*$^{+/+}$; *Sst*$^{+/-}$; and *Sst*$^{-/-}$;PER2::LUC$^{+/+}$ mice (30 weeks of age, n = 9-18/sex) were entrained to L12 and given 1µl colchicine injections 48 h prior to brain collection to analyze cumulative SCN expression of VIP, GRP, and AVP over the circadian cycle. Brains were fixed in 4% paraformaldehyde overnight, cryoprotected in 20% sucrose for 4 days, and then sectioned in the coronal plane (40µm). Free-floating slices were washed 6 times in PBS, blocked for 1 h in normal donkey serum, incubated for 48 h at 4°C with primary antibodies (Table S1), washed 6 times in PBS, incubated for 2 h at room temperature with secondary antibodies (Table S1), and then washed six times in PBS before mounting in Prolong Anti-Fade medium with DAPI (Thermo Fisher, Cat# P36935) and cover slipped. Anti-SST antibodies were validated in-house using male *Sst*$^{+/+}$ and *Sst*$^{-/-}$ mice (Figure S2A, 6-8 months old, n = 13-18/genotype, brain collection at ZT06).

Fluorescent In Situ Hybridization (FISH) and RNA Scope HiPlex

To assess RNA expression, wildtype mice (10-11 weeks of age, n = 9-11/sex) on a C57Bl/6 PER2::LUC$^{+/+}$ background were maintained under L12 in behavioral chambers for 3 weeks. Brains were collected at ZT00, ZT06, ZT12, or ZT18 (FISH: 8/sex; RNA-Scope: 7-9/sex) under bright white light or dim red light conditions dependent on ZT. Brains were rapidly dissected out, blocked to the hypothalamus, flash frozen in OCT on dry ice and stored at -80°C before sectioning. Brains were cryo-sectioned in the coronal plane (12 µm), thaw mounted onto microscope slides, and stored at -80°C until processing. For FISH, slide-mounted slices were fixed in 4% paraformaldehyde at room temperature for 60 min, washed in PBS, dehydrated through a series of 5-minute ethanol steps (50%, 70% and 100%), and dried at room temperature. Slides were processed using RNA-Scope HiPlex12 according to manufacturer instructions (Cat. No. 324140) in four successive rounds of processing and imaging. Briefly, tissue was permeabilized to allow probes to better access to the target, and target probes were hybridized to the tissue via a 2 h incubation in a humidified chamber. Hybridized probes contained a pre-amplification adapter, to which three sequential amplifier probes are attached. After hybridization and amplification steps, fluorescent detection probes are bound to the amplified probe-target complex to visualize mRNA via microscopy. After image capture of the first set of 3 probes, the subsequent 3 sets of 3 probes were processed each by gently removing coverslips, cleaving the previous fluorescent tags, and incubating with the next set before imaging. Tissue quality was confirmed via positive and negative control probes provided by company.

Microscopy and Imaging Analyses

Slices were embedded in Prolong Anti-Fade medium with DAPI (Thermo Fisher, Cat# P36935) and cover slipped. All fluorescent images were collected on a Nikon A1R+ confocal microscope (Nikon Instruments, Melville, NY, USA) or Nikon 80i microscope fitted with a Retiga 2000R digital camera (QImaging, Surrey, BC, Canada). For RNA analyses, probe image sets for each individual slice were aligned via the RNAscope Hiplex registration software 300065-USM. Protein and transcript expression was analyzed using the Analyze particles function in ImageJ software. First, images were submitted to binarized thresholding to locate cell bodies, and free-form ROIs were drawn around each brain region from which cell bodies were extracted. Since mRNA is more punctate and does not fully fill the cell body, a gaussian blur was applied before thresholding to better visualize full somas. Watershed segmentation was applied to thresholded images to further separate individual cell bodies. Average intensity values for cellular ROIs were extracted from non-thresholded images, and expression levels were quantified using background division.

Circadian behavioral assays

Mice were transferred to individual cages equipped with a running wheel, with wheel-running data collected and analyzed using ClockLab software (Actimetrics, Wilmette, IL). To test whether SST modulates photoperiodic behavior, male and female *Sst*$^{+/-}$;PER2::LUC mice, *Sst*$^{+/-}$;PER2::LUC mice and *Sst*$^{-/-}$;PER2::LUC mice (12-21 weeks; n = 3-8/genotype/photoperiod) were entrained to L12, L20, or L04 for 10 weeks. Average photophase illumination was 1107 ± 16 lux and the scotophase was completely dark. To test whether SST modulates photoperiodic after-effects, mice from Experiment 1 were released from L12, L20 and L04 into constant darkness (DD; 0 lux). After 3 weeks of free-run, mice were used to test if SST modulates the circadian resetting response to short light pulses. At times spanning the circadian cycle, mice were exposed to a 20 min light pulse (intensity: 1107 ± 16 lux). Each mouse received 3-4 light pulses separated by a minimum of 10 days to construct full photic phase response curves (PRCs) for each genotype and sex. To test whether SST affected response to simulated jetlag, male and female *Sst*$^{+/+}$ and *Sst*$^{-/-}$ mice (n = 18-21/genotype) were entrained to LD12:12 prior to a 6 h advance of the light-dark cycle. Average photophase illumination was 296 ± 0.8 lux and the scotophase was completely dark. Photophase illumination in this experiment was lower than that used in other experiments to avoid ceiling effects that high intensity light can produce in this assay (i.e., very rapid re-entrainment to the new LD cycle). Last, to test whether SST modulates parametric responses to constant

light, male and female *Sst*$^{+/+}$ and *Sst*$^{-/-}$ mice (n = 7-16/genotype/sex) were transferred from L12 into constant light (LL) for 8-13 weeks. Average LL illumination was 1215 ± 25 lux.

Genotype differences in circadian phase, waveform, period, and photic resetting was assessed. To quantify circadian waveform under L12, L20, and L04 conditions, the duration of the behavioral active phase (i.e., alpha) was measured by the difference between locomotor activity offset and onset on each day of the experiment. Phase angle of entrainment was calculated using activity onset. To quantify masking under L20, the proportion of activity during the scotophase and the 4 hours before and after the scotophase were quantified. The architecture of nighttime activity patterns was assessed by quantifying duration and consistency of non-active bouts during the scotophase ("siestas") using Average Activity profiles for consecutive 2-week intervals during entrainment. Under DD, free-running period length was calculated using the slope of the linear regression fit to the first 7 consecutive activity onsets after release. In addition, alpha was quantified daily for the first 7-10 days of DD and averaged weekly over the first 3 weeks of DD. To compare alpha change across sex and genotype, DD alpha was normalized to alpha in the week prior to DD. To construct the photic PRC, phase resetting was quantified by calculating the difference between linear regression lines fit to 4 consecutive activity onsets before and after each light pulse. Recovery from simulated jetlag was quantified for each mouse by calculating the number of days required for activity onsets to advance by 6 h (i.e., align to new lights off). Last, lack of rhythmicity under LL was quantified by visual inspection and χ^2 periodogram analyses.

PER2::LUC Tissue Collection, Recording, and Analyses

Mice were anesthetized with isoflurane and sacrificed using cervical dislocation 4-6 h before lights off to minimize dissection-induced resetting, as in previous work (13). SCN slices (150 μm) were collected in the coronal plane using a vibratome (Leica VT1200S) and trimmed by hand under a dissecting microscope. SCN slices were cultured at 37˚C on a membrane insert in a dish containing 1.2mL of air-buffered Dulbecco's modified explant medium (DMEM, Sigma D2902) supplemented with 0.1mM beetle luciferin, 0.02% B27 (Gibco 17504), 0.01% HEPES (Gibco 15630), 0.005% $NaCHO_3$ (Gibco 25080), 0.004% Dextrose (Sigma G7021), and 0.01% penicillin/streptomycin (Gibco 15140). To test effects of SSTR1 signaling, the selective SSTR1 agonist CH275 (1μM, Tocris Cat#2454) or volume-matched vehicle (DMEM, 3μl) was applied directly to each SCN slice at ZT12. PER2::LUC rhythms were monitored for at least 4 days with luminometry (Actimetrics, LumiCycle 32). To test SCN photoperiodic responses, mice were entrained to L12 or L20 for at least 4 weeks. PER2::LUC SCN slices were cultured with or without a broad spectrum SSTR antagonist (20uM, Tocris Cat#3493) for the duration of the experiment. Bioluminescence rhythms were imaged using a Stanford Photonics XR Mega 10z CCD camera mounted onto a Zeiss Axio Observer Z1 microscope controlled with Piper software (Stanford Photonics). Images (1.4k×1k 16-bit) were collected at 15 frames/sec, filtered in real-time to eliminate single-image noise events (i.e., cosmic rays), and stored as 2 min-summed images collected once every 15 min. A 2 h moving average was then applied (Piper Software), images were converted to 8-bit, pixel dimensions were reduced in half, and two consecutive images were summed to produce a series of 30 min images (ImageJ Software). For luminometry and imaging analyses, recording start time was normalized for each sample to the ZT start of recording. For luminometry, the PER2::LUC time series was detrended and analyzed with Lumicycle software by fitting a damped sine wave to the first 4 full cycles in vitro (LM Fit – smoothing 6). Goodness of fit, period, and damping rate (i.e., number of days for rhythm amplitude to decrease about 37%) was recorded from the sine fit. In addition, daily times and values of peak and trough PER2::LUC were recorded to calculate cycle-to-cycle amplitude (peak – trough) and average period. For imaging data, Matlab-based computational analyses were used as described previously (4).

Statistical analyses

Data are represented in Figures as Mean ± SEM. Cosine curve-fitting was performed to detect significant daily rhythms using Circwave software (56). Other statistical analyses were performed with JMP software

(SAS Institute, Cary, NC). When models contained within-subject factors (Region, Slice Position, Weeks), a mixed linear model was used to parse out random effects driven by individual differences among mice. When models only contained between-subject factors, a full-factorial ANOVA was used to assess the effects and interactions of one to four factors: 1) SST Genotype, 2) Photoperiod, 3) Time of Day, and/or 4) Sex. Data were analyzed for each sex separately where appropriate. Post-hoc tests were performed with Tukey's HSD or Least Square Mean contrasts to control for family-wise error. Statistical significance was set at $p < 0.05$.

References

1. Taniguchi H (2014) Genetic dissection of GABAergic neural circuits in mouse neocortex. *Frontiers in cellular neuroscience* 8.
2. Madisen L*, et al.* (2010) A robust and high-throughput Cre reporting and characterization system for the whole mouse brain. *Nat Neurosci* 13(1):133-140.
3. Harris JA*, et al.* (2014) Anatomical characterization of Cre driver mice for neural circuit mapping and manipulation. *Frontiers in neural circuits* 8:76.
4. Evans JA, Leise TL, Castanon-Cervantes O, & Davidson AJ (2013) Dynamic interactions mediated by nonredundant signaling mechanisms couple circadian clock neurons. *Neuron* 80(4):973-983.

Table S1 – Immunohistochemistry antibodies

Antigen/ Antibody	RRID	Species (nm)	Dilution	Source	Catalog #
SST (1º)	AB_518614	Rabbit	1:1K	BMA/ Peninsula	T-4103.0050
VIP (1º)	AB_518682	Rabbit	1:500	BMA/ Peninsula	T-4246
AVP (1º)	AB_518680	Guinea pig	1:500	BMA/ Peninsula	T-5048
GRP (1º)	AB_519013	Rabbit	1:1K	BMA/ Peninsula	T-4351
Rabbit (2º)	AB_2313584	Donkey (488)	1:500	Jackson	711-545-152
Guinea Pig (2º)	AB_2340476	Donkey (647)	1:500	Jackson	706-605-148

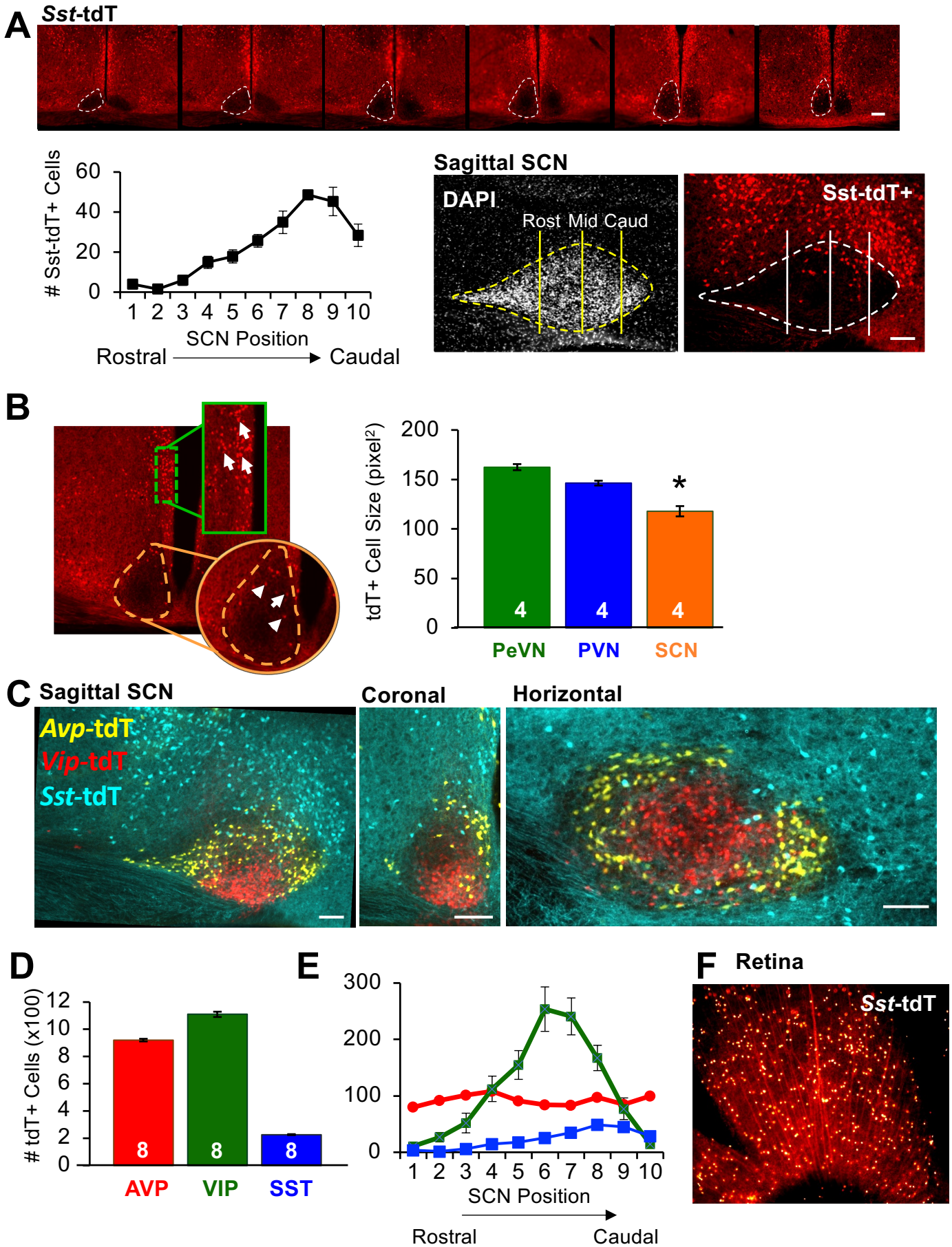
A
Sst-tdT
Sst-tdT+ Cells
60
40
20
0
1 2 3 4 5 6 7 8 9 10
SCN Position
Rostral
Caudal
Sagittal SCN
DAPI
Rost Mid Caud
Sst-tdT+
B
tdT+ Cell Size (pixel²)
200
150
100
50
0
4
4
4
*
PeVN
PVN
SCN
C
Sagittal SCN
Avp-tdT
Vip-tdT
Sst-tdT
Coronal
Horizontal
D
tdT+ Cells (x100)
12
10
8
6
4
2
0
8
8
8
AVP
VIP
SST
E
300
200
100
0
1 2 3 4 5 6 7 8 9 10
SCN Position
Rostral
Caudal
F
Retina
Sst-tdT

FigureS1

Figure S1. Spatial mapping of Sst cells in the SCN. A) Sst-tdT expression across the anteroposterior SCN in the coronal and sagittal planes. B) Comparison of Sst-tdT cell size in the hypothalamus. C) DAPI-aligned, superimposed images of SCN slices taken from *Sst*- *Vip*- and *Avp*-tdT cells. D-E) Comparison of *Sst*-, *Vip-,* and *Avp*-tdT cell numbers. F) Retinal expression of *Sst*-tdT. Scale bars = 100μm, * post hoc comparisons, $p < 0.05$.

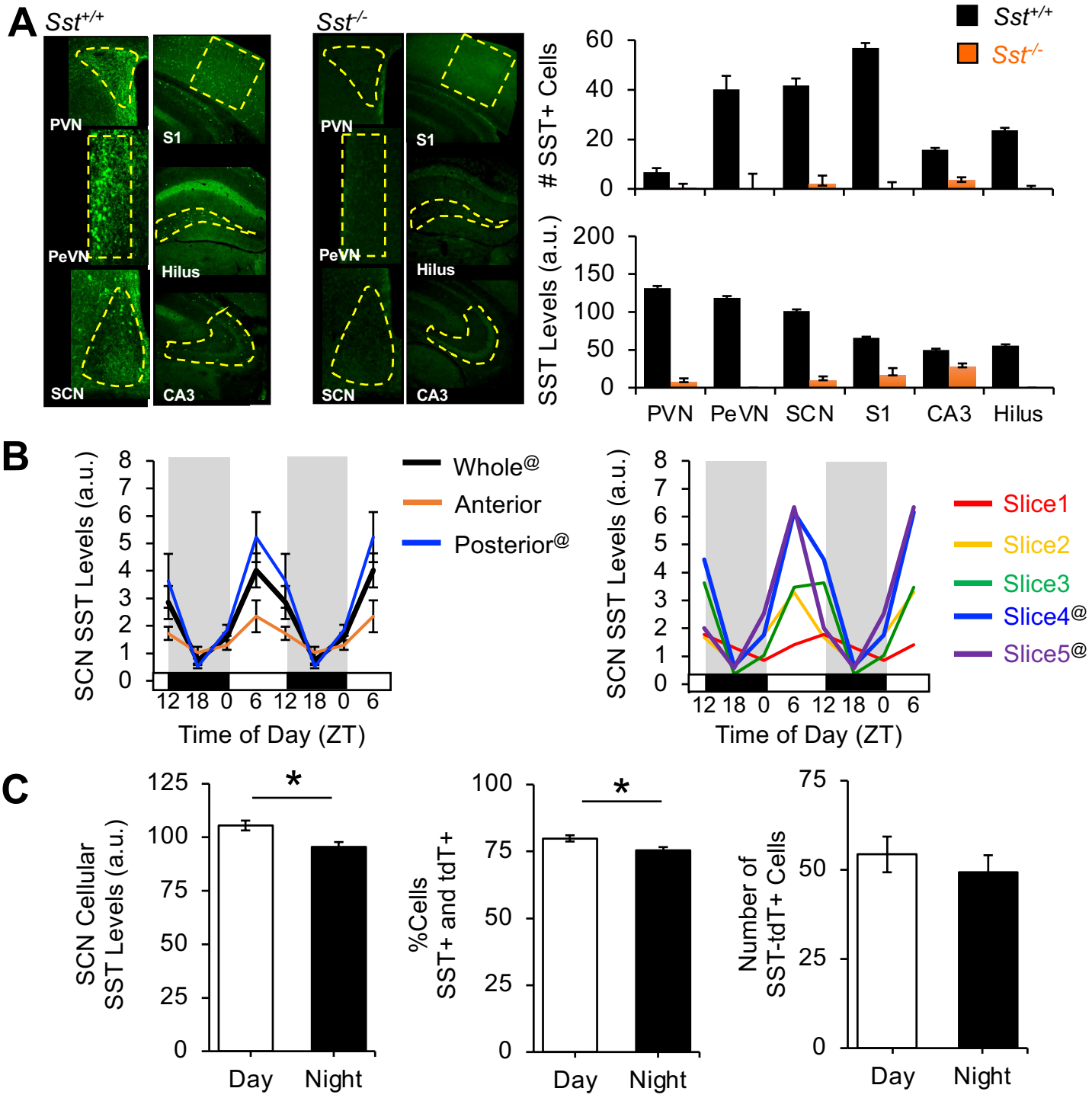
A
Sst+/+
Sst-/-
PVN
PeVN
SCN
S1
Hilus
CA3
SST+ Cells
SST Levels (a.u.)
PVN PeVN SCN S1 CA3 Hilus
B
SCN SST Levels (a.u.)
Time of Day (ZT)
Whole@
Anterior
Posterior@
Slice1
Slice2
Slice3
Slice4@
Slice5@
C
SCN Cellular SST Levels (a.u.)
%Cells SST+ and tdT+
Number of SST-tdT+ Cells
Day
Night

FigureS2

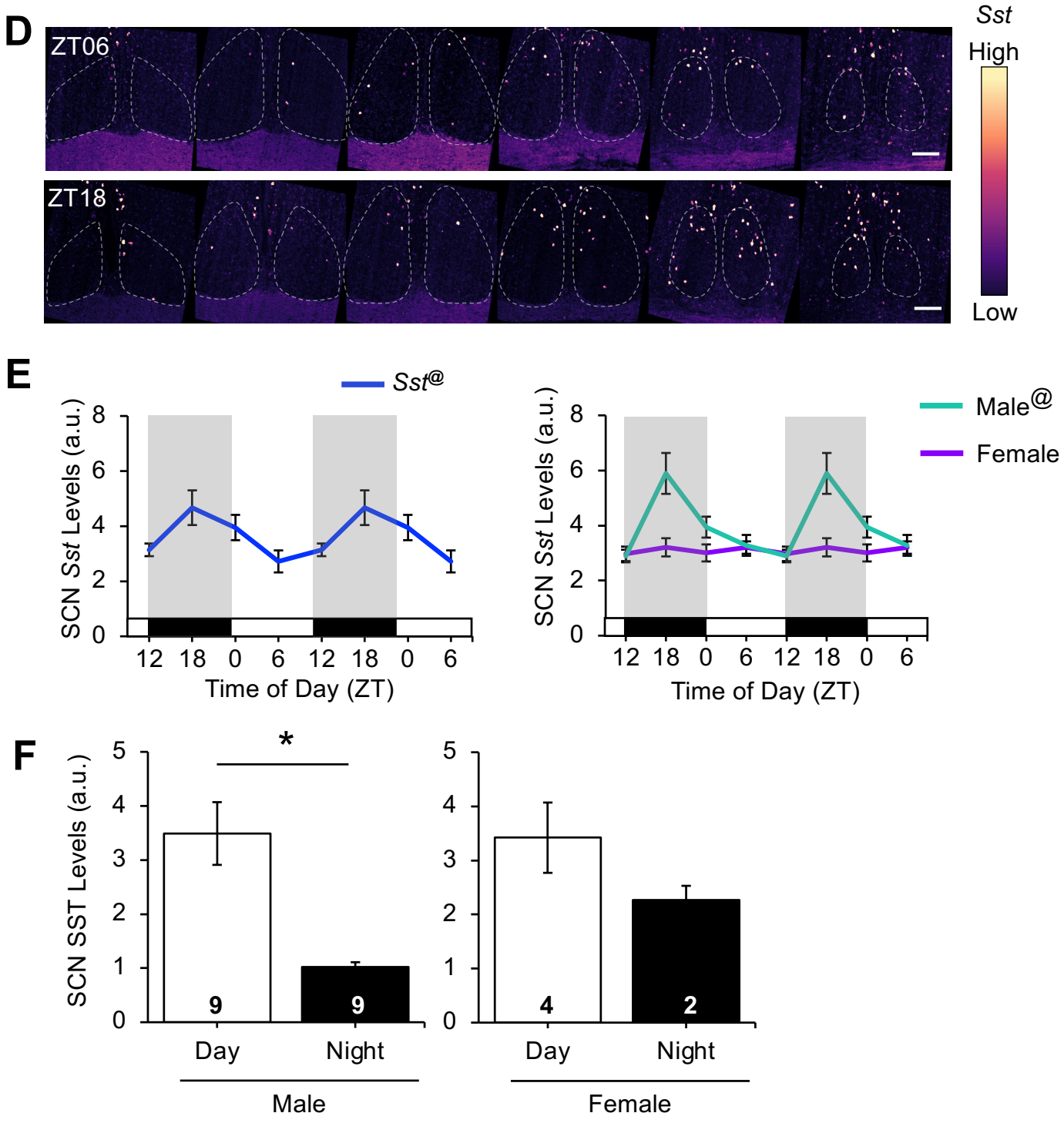

FigureS2 cont

Figure S2. SCN expression of SCN SST/*Sst* is rhythmic and differs by sex. A) Antibody validation. Relative to wildtype mice, SST was significantly lower in *Sst*$^{-/-}$ mice in each structure examined. B) SCN SST-IHC+ expression in LD12:12, double-plotted to facilitate visualization. SCN SST rhythms were significant in posterior SCN slices (Circwave: Caudal SCN: $F(2,21) = 7.8$, $p = 0.003$; Rostral SCN: $F(2,19) = 0.62$, $p > 0.5$). C) Day-night variation in SST, SST+*Sst*-tdT labeling, but not *Sst*-tdT labeling alone in the SCN. D) Representative images illustrating *Sst*+ cells in the anteroposterior SCN. E) SCN *Sst* expression in LD12:12, double-plotted to facilitate visualization. *Sst* transcription was rhythmic in males, but not females (Males- $F(3,98) = 9.8$, $p = 0.0001$, Females- $F(3,113) = 0.0$, $p > 0.9$). F) Day-night SST expression varied in male SCN, but not female SCN (Males: $t(16) = 2.75$, $p < 0.05$, Females: $t(4) = 1.38$, $p > 0.2$). Scale bars = 100μm, ZT = Zeitgeber Time, a.u. = arbitrary units. [@]Circwave test of rhythmicity, $p < 0.05$. * post hoc comparisons, $p < 0.05$.

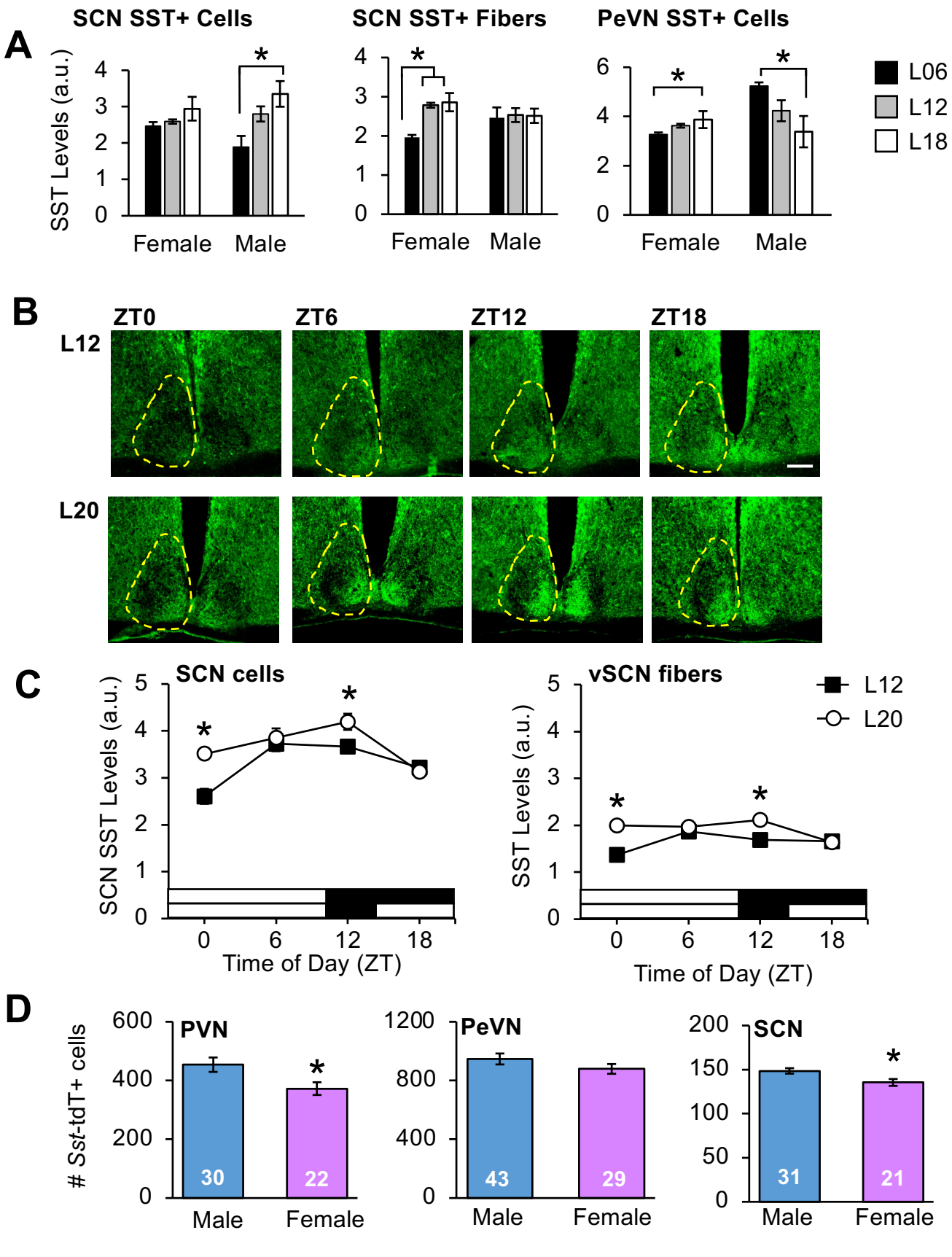
A
SCN SST+ Cells
SCN SST+ Fibers
PeVN SST+ Cells
SST Levels (a.u.)
Female
Male
L06
L12
L18
B
ZT0
ZT6
ZT12
ZT18
L12
L20
C
SCN cells
vSCN fibers
SCN SST Levels (a.u.)
SST Levels (a.u.)
L12
L20
Time of Day (ZT)
Time of Day (ZT)
D
Sst-tdT+ cells
PVN
PeVN
SCN
30
22
43
29
31
21
Male
Female

FigureS3

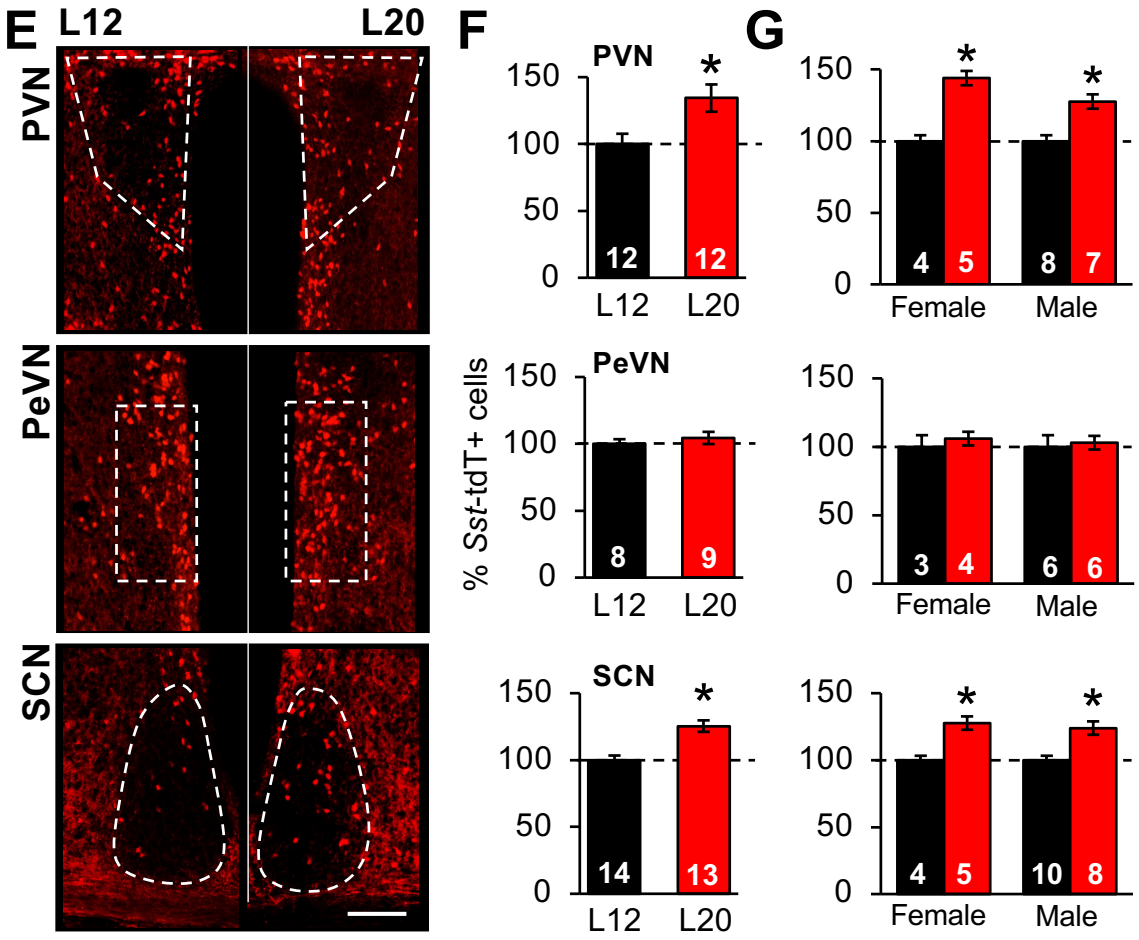

FigureS3 cont

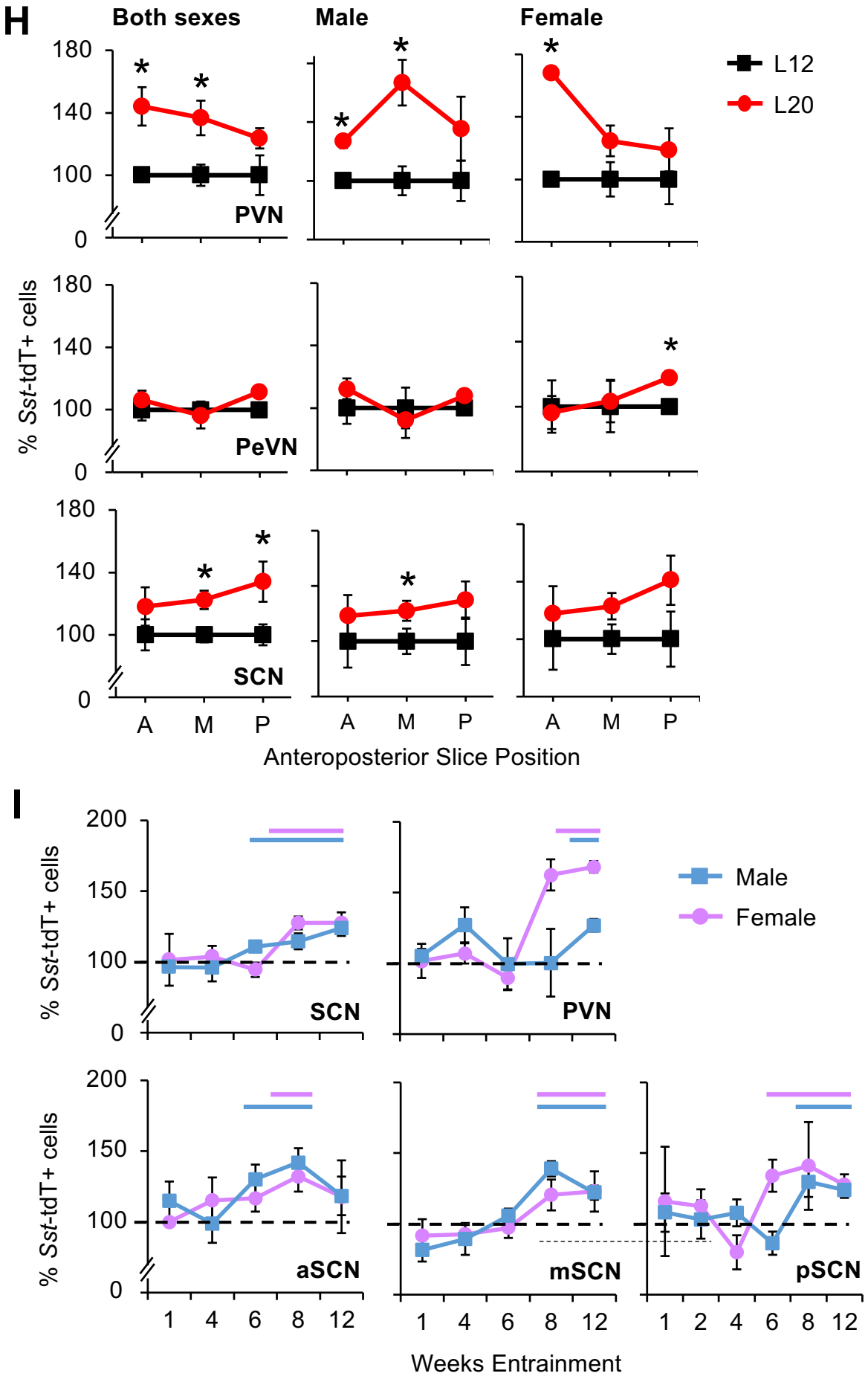

FigureS3 cont

Figure S3. Photoperiodic modulation of SCN SST/*Sst*-tdT expression. A) Mice were entrained to short (L06), control (L12), or long day photoperiods (L18). Mice received 1µl colchicine into the third ventricle 48 h prior to brain collection to slow microtubule transport and visualize total peptide production over the circadian cycle. In the SCN, SST levels were proportional to day length, which varied by sex (PP: $F(2,17) = 7.8$, $p = 0.004$, Sex: $F(1,17) < 0.1$, $p > 0.9$, PP*Sex: $F(2,17) = 2.3$, $p > 0.1$). In the PeVN, SST also varied with photoperiod and was influenced by sex ($F(2,17) = 0.2$, $p = 0.8$, Sex: $F(1,17) = 6.5$, $p = 0.02$, PP*Sex: $F(2,17) = 7.0$, $p = 0.006$). B-C) Male mice were entrained to L20 (13). L20 increased SST expression at the time of dawn and dusk under control conditions in both SCN cells (Cells: PP: $F(1,90) = 2.7$, $p = 0.01$, ZT: $F(3,90) = 8.6$, $p < 0.0001$, PP*ZT: $F(3,90) = 4.4$, $p = 0.006$) and fiber-like processes in the SCN core (PP: $F(1,90) = 42.8$, $p < 0.0001$, ZT: $F(3,90) = 10.6$, $p < 0.0001$, PP*ZT: $F(3,90) = 11.9$, $p < 0.0001$). D) Sex influenced number of *Sst*-tdT+ cells in L12 mice (SCN: $F(1,42) = 2.6$, $p < 0.05$; PVN: $F(1,50) = 2.5$, $p < 0.05$; PeVN: $F(1,70) = 1.4$, $p > 0.1$). E) Representative images illustrating *Sst*-tdT cell populations in each hypothalamic region. F-G) Twelve weeks of L20 entrainment increased the number of *Sst*-tdT+ cells in the PVN and SCN. H) Regional patterns of L20-induced *Sst*-tdT expression in the SCN, PeVN, and PVN. I) L20-induced *Sst*-tdT expression in the SCN and PVN of each sex. Color-coded lines indicate timepoints where L20-induced increase is greater than 0. Scale bars = 100µm, ZT = Zeitgeber Time, a.u. = arbitrary units. A, M, P = Anterior, Middle, and Posterior slices of each structure. * post hoc comparisons, $p < 0.05$.

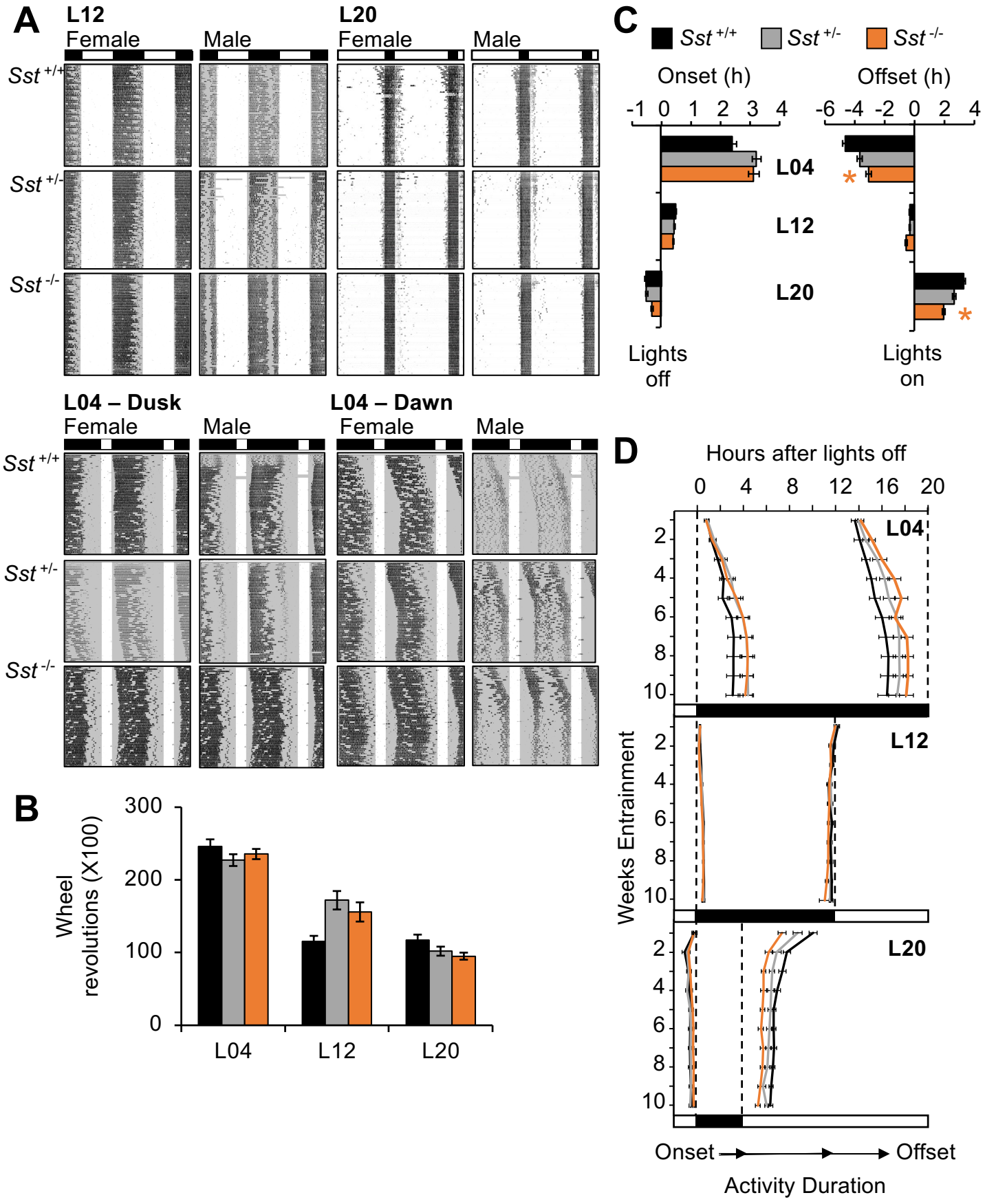
A
L12
Female
Male
L20
Female
Male
Sst +/+
Sst +/-
Sst -/-
L04 – Dusk
Female
Male
L04 – Dawn
Female
Male
Sst +/+
Sst +/-
Sst -/-
B
Wheel revolutions (X100)
300
200
100
0
L04
L12
L20
C
Sst +/+
Sst +/-
Sst -/-
Onset (h)
-1 0 1 2 3 4
Offset (h)
-6 -4 -2 0 2 4
L04
L12
L20
Lights off
Lights on
D
Hours after lights off
0 4 8 12 16 20
L04
L12
L20
Weeks Entrainment
2 4 6 8 10
Onset
Offset
Activity Duration

FigureS4

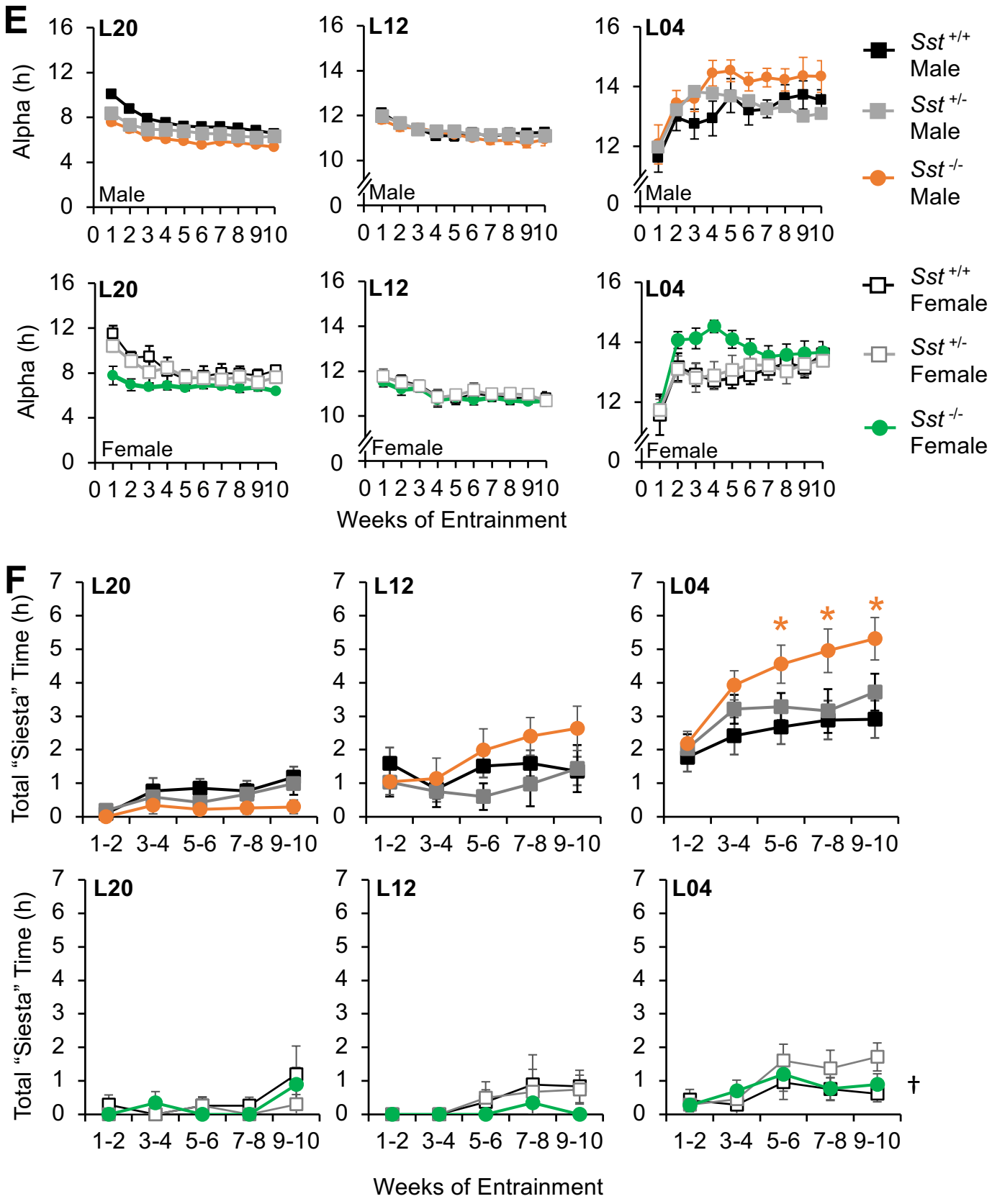

FigureS4 cont

G

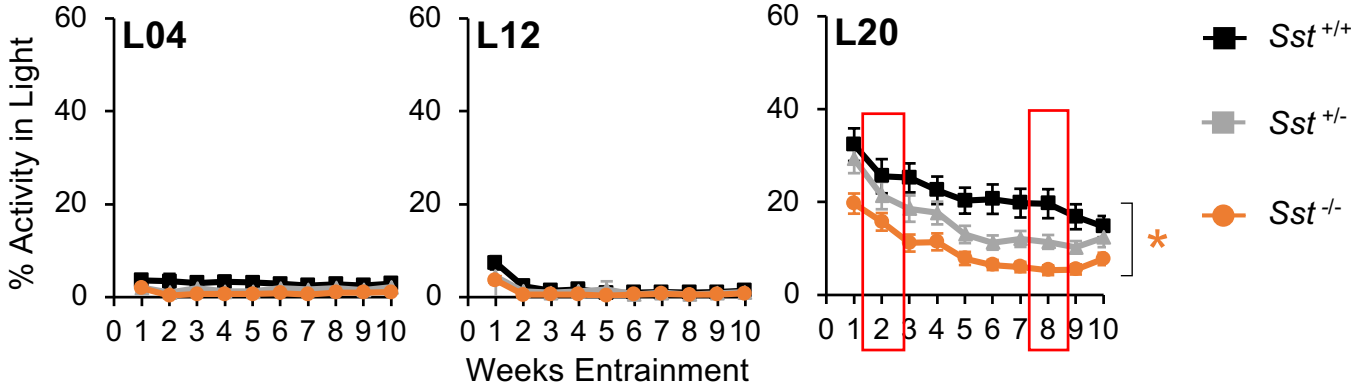

H

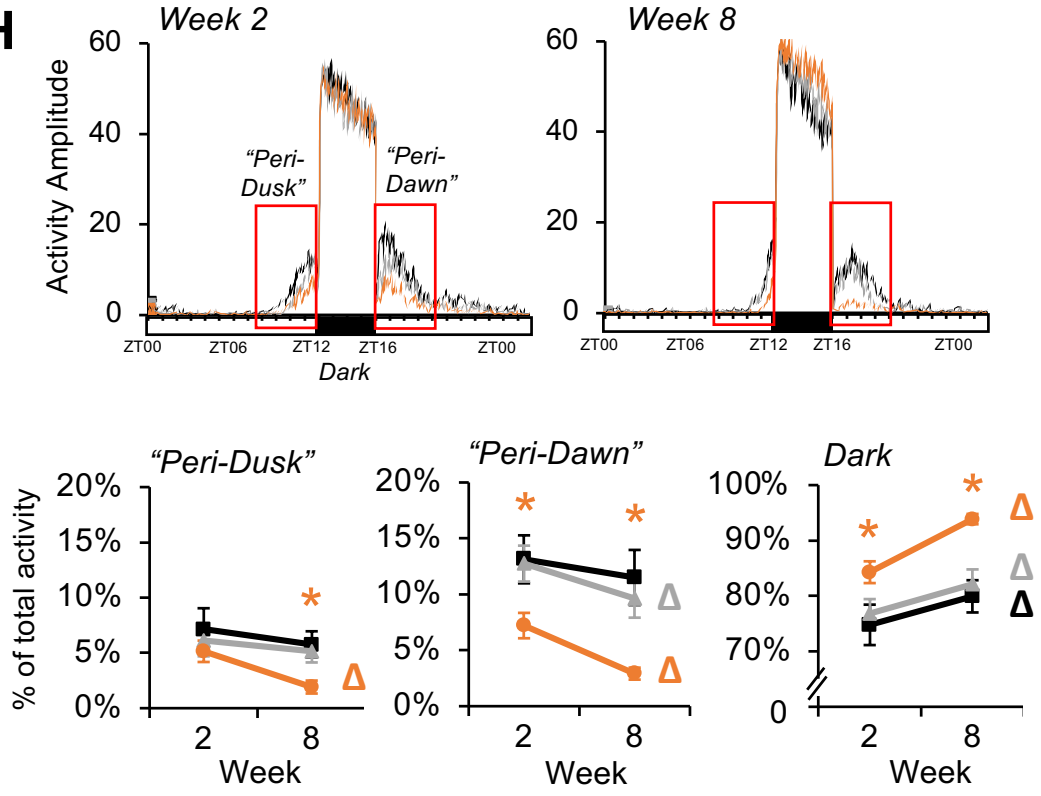

FigureS4 cont

Figure S4. Lack of SST enhances photoperiodic modulation of circadian rhythms.
A) Representative double-plotted, wheel-running actograms from each sex and photoperiod. B) Activity levels across photoperiod did not differ by genotype (L20- GT: $F(2,50) = 0.4$, $p > 0.6$, Week: $F(9,450) = 17.7$, $p < 0.0001$; GT*Week: $F(18,450) = 0.7$, $p > 0.8$; L04- GT: $F(2,55) = 0.2$, $p > 0.8$, Week: $F(9,495) = 29.5$, $p < 0.0001$; GT*Week: $F(18,495) = 1.6$, $p < 0.05$; L12- GT: $F(2,50) = 0.5$, $p > 0.5$, Week: $F(9,396) = 25.0$, $p < 0.0001$; GT*Week: $F(18,396) = 0.7$, $p > 0.7$).
C) Phase angle of entrainment for activity offset differed by genotype in L20 and L04, but not L12 (L20- GT: $F(2,50) = 11.9$, $p < 0.0001$; GT*Week: $F(18,450) = 2.8$, $p = 0.0001$, Week: $F(9,450) = 66.6$, $p < 0.0001$; L04- GT: $F(2,55) = 3.2$, $p = 0.05$; Week: $F(9,495) = 47.9$, $p < 0.0001$, GT*Week: $F(18,495) = 0.8$, $p > 0.6$; L12- GT: $F(2,44) = 1.73$, $p > 0.1$; Week: $F(9,396) = 9.16$, $p < 0.0001$; GT*Week: $F(18,396) = 0.8$, $p > 0.5$). Activity onset did not differ by genotype in any photoperiod (L20- GT: $F(2,50) = 1.5$, $p > 0.2$; GT*Week: $F(18,450) = 0.9$, $p > 0.5$, Week: $F(9,450) = 12.5$, $p < 0.0001$; L04- GT: $F(2,40) = 1.4$, $p > 0.2$; GT*Week: $F(18,495) = 1.3$, $p > 0.2$, Week: $F(9,495) = 63.7$, $p < 0.0001$; L12- GT: $F(2,44) = 0.6$, $p > 0.5$; Week: $F(9,396) = 29.02$, $p < 0.0001$; GT*Week: $F(18,396) = 0.5$, $p > 0.8$). D) Vertical plot illustrating changes in activity onset, offset, and alpha under each week of photoperiodic entrainment (L20 Alpha- GT: $F(2,50) = 20.0$, $p < 0.0001$, Week: $F(9,450) = 59.9$, $p < 0.0001$; GT*Week: $F(18,450) = 2.3$, $p = 0.002$; L04 Alpha- GT: $F(2,55) = 3.5$, $p = 0.04$, Week: $F(9,495) = 24.6$, $p < 0.0001$; GT*Week: $F(18,495) = 1.5$, $p = 0.08$; L12 Alpha- GT: $F(2,44) = 0.5$, $p > 0.5$, Week: $F(9,396) = 24.9$, $p < 0.0001$; GT*Week: $F(18,396) = 0.6$, $p = 0.08$). E) Effects of genotype on photoperiodic changes in alpha divided by sex (L20 Males- GT: $F(1,28) = 45.1$, $p < 0.0001$; GT*Week: $F(9,252) = 2.0$, $p = 0.04$, Week: $F(9,252) = 41.1$, $p < 0.0001$; L20 Females- Week: $F(9,45) = 8.2$, $p < 0.0001$, GT*Week: $F(9,45) = 8.2$, $p = 0.004$, GT: $F(1,5) = 7.3$, $p = 0.04$; L04 Males- GT: $F(1,14) = 2.2$, $p > 0.1$; Week: $F(9,126) = 13.4$, $p < 0.0001$, GT*Week: $F(9,126) = 0.71$, $p > 0.6$; L04 Females- GT: $F(1,17) = 4.2$, $p = 0.05$; Week: $F(9,153) = 9.0$, $p < 0.0001$, GT*Week: $F(9,153) = 2.12$, $p = 0.03$; L12 Males- GT: $F(1,20) = 0.6$, $p > 0.4$; Week: $F(9,180) = 12.0$, $p < 0.0001$; GT*Week: $F(18,180) = 1.28$, $p > 0.2$; L12 Females- GT: $F(1,9) = 0.32$, $p > 0.5$; Week: $F(9,81) = 4.11$, $p = 0.0002$; GT*Week: $F(9,81) = 0.13$, $p > 0.8$) F) Photoperiodic modulation of daily amount of scotophase inactivity (i.e., "siesta") divided by sex and photoperiod. G) Percent of daily activity during the photophase divided by genotype and photoperiod. Photophase activity under L20 was lower in S$s t^{-/-}$ mice and decreased in all mice over time (GT: $F(2,47) = 6.9$, $p < 0.005$; Week: $F(9,423) = 129.5$, $p < 0.0001$; Sex: $F(1,47) = 1.0$, $p > 0.3$; GT*Sex*Week: $F(18,423) = 1.0$, $p > 0.4$). Under L04 and L12, photophase activity was influenced by sex and entrainment week, but not genotype (L04- Sex: $F(1,52) = 7.6$, $p < 0.01$; Week: $F(9,468) = 2.1$, $p < 0.05$; GT: $F(2,52) = 2.5$, $p = 0.09$; GT*Sex*Week: $F(18,468) = 1.3$, $p > 0.1$; L12- Sex: $F(1,41) = 4.8$, $p < 0.05$; Week: $F(9,369) = 14.8$, $p < 0.0001$; GT: $F(2,41) = 1.2$, $p > 0.3$; GT*Sex*Week: $F(18,369) = 0.3$, $p > 0.9$). After 2 and 8 weeks of L20 entrainment, changes in peri-dusk and -dawn activity levels corresponded with increased scotophase activity (Peri-dusk- GT: $F(2,51) = 2.2$, $p > 0.1$; Wk: $F(1,51) = 4.5$, $p < 0.05$; GT*Wk: $F(2,51) = 0.6$, $p > 0.5$; Peri-dawn- GT: $F(2,51) = 5.6$, $p < 0.01$; Wk: $F(1,51) = 16.1$, $p < 0.0005$; GT*Wk: $F(2,51) = 1.1$, $p > 0.3$; Dark- GT: $F(2,51) = 6.9$, $p < 0.005$; Wk: $F(1,51) = 24.3$, $p < 0.0001$; GT*Wk: $F(2,51) = 1.2$, $p > 0.3$). †Wildtype sex difference, *Genotype difference, $^{\Delta}$Week 2-to-8 difference; post hoc comparisons, $p < 0.05$.

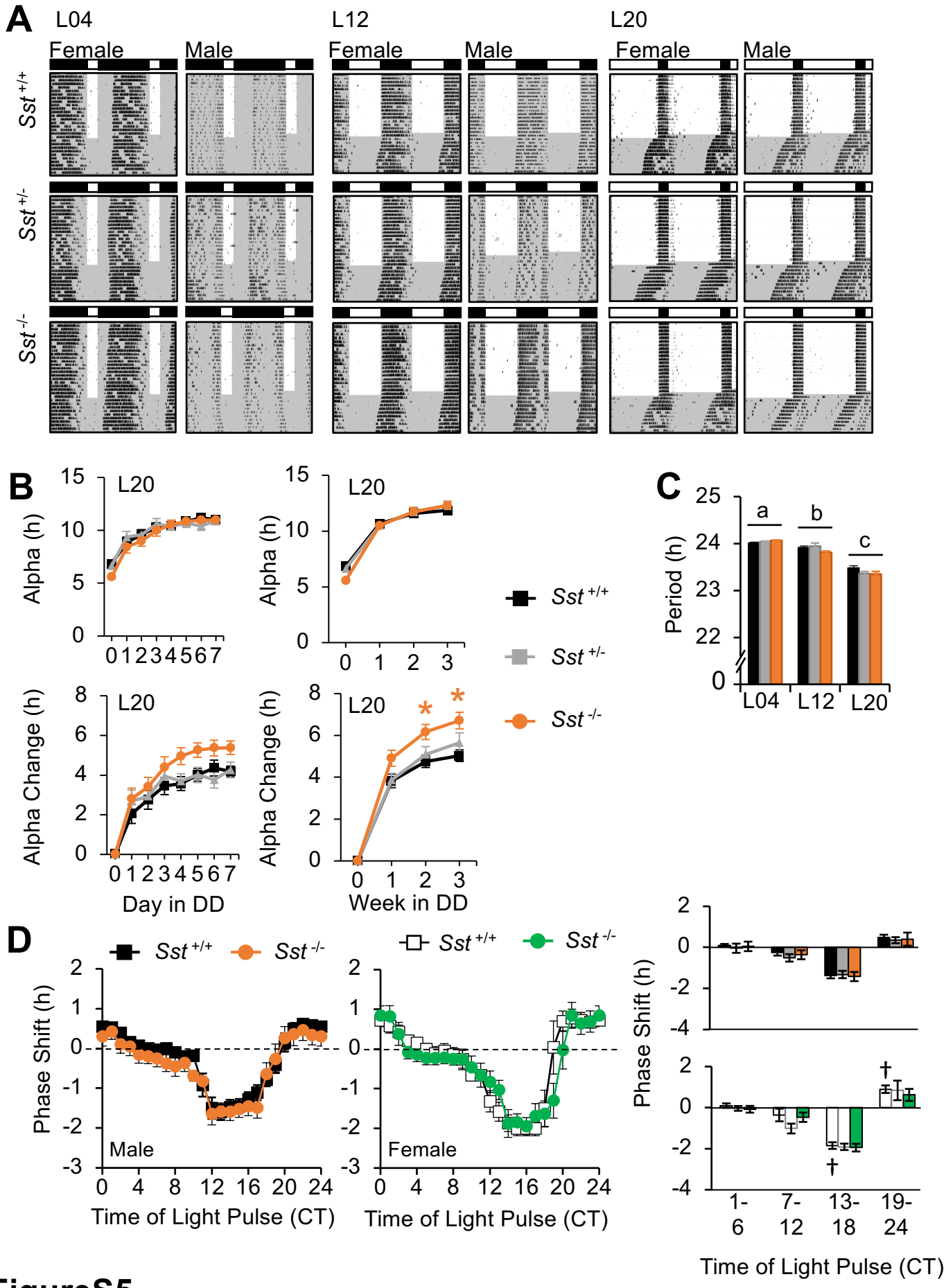
A
L04
L12
L20
Female
Male
Sst +/+
Sst +/-
Sst -/-
B
L20
Alpha (h)
Alpha Change (h)
Day in DD
Week in DD
C
Period (h)
a
b
c
L04
L12
L20
D
Phase Shift (h)
Male
Female
Time of Light Pulse (CT)
1-6
7-12
13-18
19-24

FigureS5

Figure S5. Lack of SST modulated circadian waveform after DD release, but not circadian period or photic resetting. A) Representative actograms illustrating release from DD in each photoperiod. B) Lack of SST influenced changes in alpha after DD release from L20 (L20: GT: $F(2,40) = 5.2$, $p < 0.01$; Week: $F(2,80) = 90.1$, $p < 0.0001$; GT*Week: $F(2,80) = 1.5$, $p > 0.2$, L12: - GT: $F(2,30) = 0.3$, $p > 0.7$; Week: $F(2,60) = 8.9$, $p < 0.0005$; GT*Week: $F(2,60) = 0.4$, $p > 0.8$; L04- GT: $F(2,81) = 0.4$, $p > 0.6$; Week: $F(2,162) = 2.6$, $p = 0.08$; GT*Week: $F(2,162) = 0.9$, $p > 0.4$). C) Photoperiodic after-effects in circadian period (PP: $F(2,151) = 285.42$, $p < 0.0001$). Overall, wildtype $Sst^{+/+}$ mice displayed longer periods relative to other groups (GT: $F(2,151) = 2.13$, $p > 0.1$; PP*GT: $F(4,151) = 3.2$; $p < 0.02$), but there was no genotype effect when parsed by photoperiod (L12: $F(2,30) = 2.1$, $p > 0.1$; L20: $F(2,40) = 1.9$, $p > 0.1$; L04: $F(2,81) = 2.1$, $p > 0.1$). D) Photic resetting differed by sex (Sex: $F(1,292) = 4.9$, $p = 0.05$; CT: $F(3,292) = 157.2$, $p < 0.0001$; Sex*CT: $F(3,292) = 6.4$, $p < 0.0005$) but not genotype or photoperiod (GT: $F(2,292) = 1.9$, $p > 0.1$; PP: $F(2,292) = 1.4$, $p > 0.2$; GT*PP: $F(4,292) = 1.5$, $p > 0.2$; GT*CT: $F(6,292) = 0.6$, $p > 0.7$; Sex*PP: $F(2,292) = 0.5$, $p > 0.6$; GT*Sex: $F(2,292) = 0.9$, $p > 0.4$). †Wildtype sex difference, *Genotype difference, post hoc comparisons, $p < 0.05$.

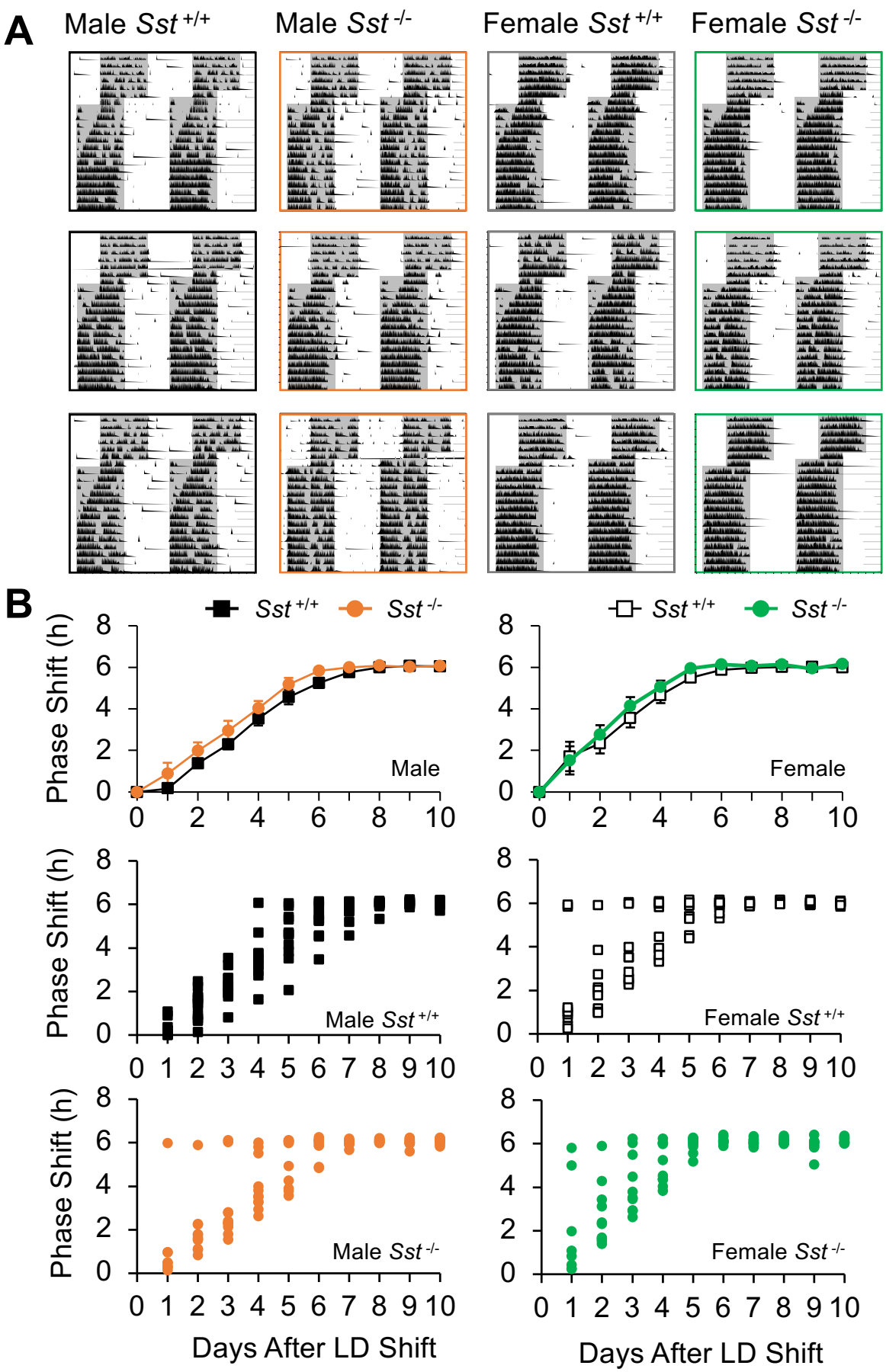
A
Male Sst +/+
Male Sst -/-
Female Sst +/+
Female Sst -/-
B
Sst +/+
Sst -/-
Phase Shift (h)
Male
Female
Male Sst +/+
Female Sst +/+
Male Sst -/-
Female Sst -/-
Days After LD Shift

FigureS6

Figure S6. Lack of SST accelerates jetlag recovery. A). Representative double-plotted wheel running actograms illustrating re-entrainment to a 6-h advance of the L12 light:dark cycle in each group. A). Day-to-day onsets, summarized by group (top) and plotted for individual mice (bottom).

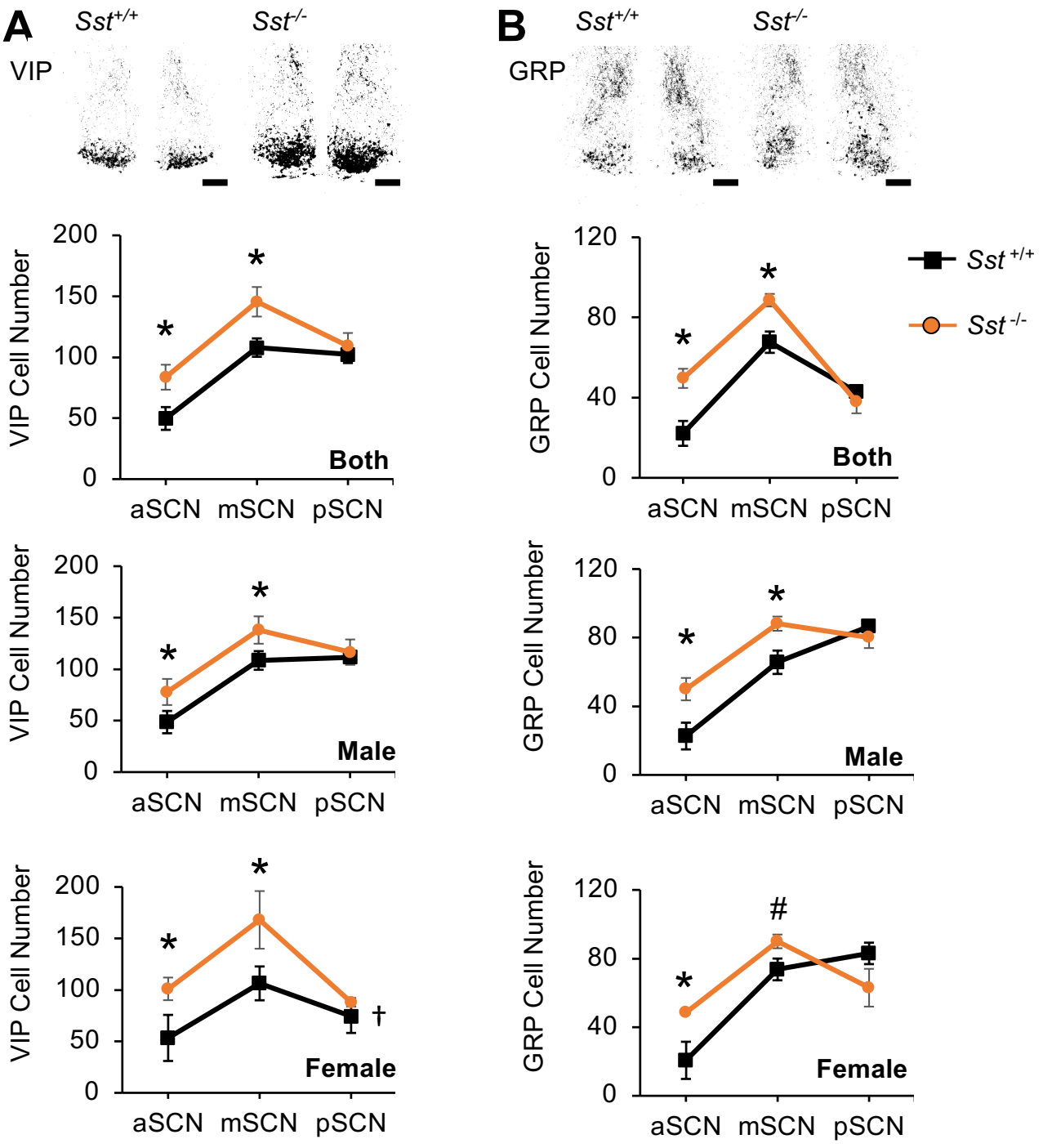
A
Sst+/+
Sst-/-
VIP
VIP Cell Number
200
150
100
50
0
aSCN mSCN pSCN
Both
Male
Female
*
†
B
GRP
GRP Cell Number
120
80
40
0
#
Sst +/+
Sst -/-

FigureS7

Figure S7. Lack of SST affects VIP and GRP cell populations in specific SCN subregions. Relative to controls, knockout *Sst*$^{-/-}$ mice displayed increased VIP- and GRP-expressing cells in the anterior and middle SCN, but did not differ in the number of VIP and GRP cells in the posterior SCN. Scale bars = 100μm, * post hoc comparisons, $p < 0.05$.

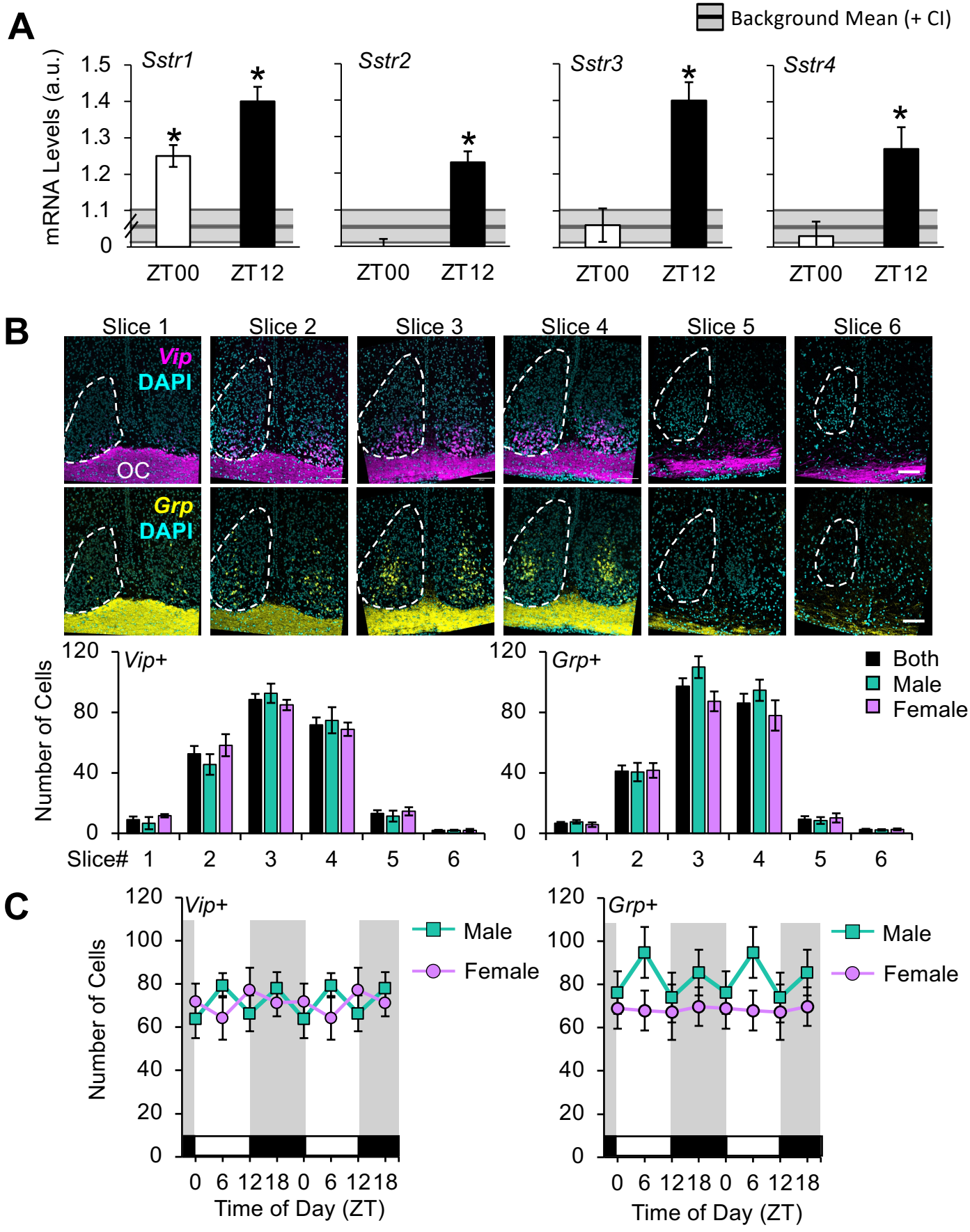
A
Background Mean (+ CI)
mRNA Levels (a.u.)
Sstr1
Sstr2
Sstr3
Sstr4
ZT00
ZT12
B
Slice 1
Slice 2
Slice 3
Slice 4
Slice 5
Slice 6
Vip
DAPI
OC
Grp
DAPI
Number of Cells
Vip+
Grp+
Both
Male
Female
Slice# 1 2 3 4 5 6
C
Vip+
Grp+
Male
Female
Number of Cells
Time of Day (ZT)

FigureS8

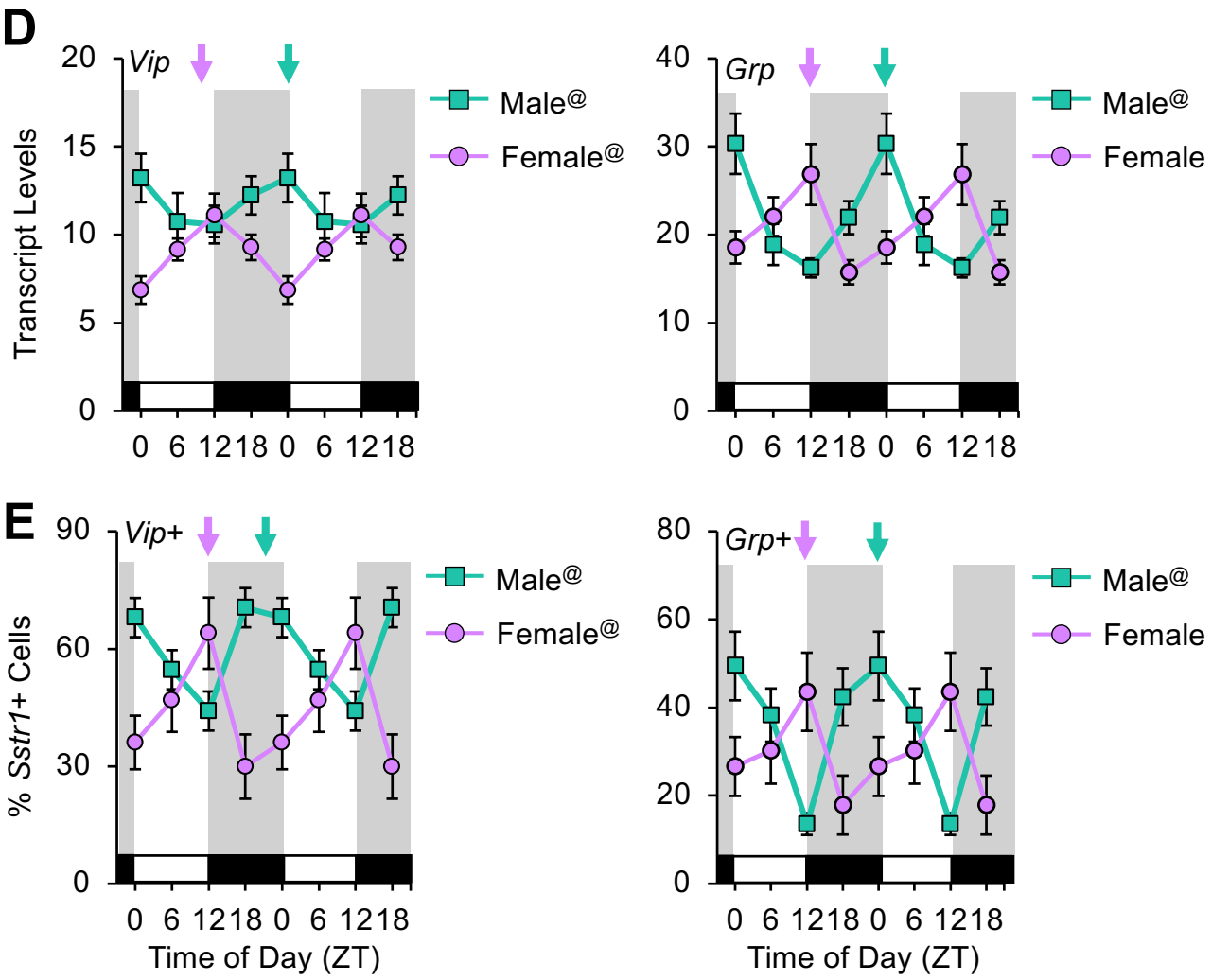

FigureS8 cont

Figure S8. SCN expression of *Sstr*, *Vip*, and *Grp*. A) Each SST receptor displayed modest day night differences (*Sstr1*- $t(43) = 2.7$, $p = 0.009$; *Sstr2*- $t(42) = 6.3$, $p < 0.001$; *Sstr3*- $t(45) = 5.6$, $p < 0.0001$; *Sstr4*- $t(42) = 3.3$, $p < 0.002$). B) Representative images of *Vip*+ and *Grp*+ cells, with quantification of cell number across the anteroposterior SCN. As expected, most cells of each type in each sex were located in Slice2-4, which were used for analyses. C) The number of *Vip* and *Grp* SCN neurons detected with RNAScope did not differ across time of day (*Vip*- Male- $F(2,51) = 0.1$, $p > 0.9$, Female- $F(2,61) = 0.4$, $p > 0.6$; *Grp*- Male- $F(2,51) = 0.2$, $p > 0.8$, Female- $F(2,61) = 0.1$, $p > 0.8$). D) *Vip* and *Grp* transcription was rhythmic in manner that differed by sex (*Vip*- Male- $F(2,51) = 4.9$, $p < 0.05$, Female- $F(2,61) = 6.6$, $p < 0.005$; *Grp*- Male- $F(2,51) = 11.2$, $p < 0.001$, Female- $F(2,61) = 3.4$, $p < 0.05$). E) Percentage of *Vip*+ and *Grp*+ neurons with *Sstr1* expression 150% above background was rhythmic but varied by sex (*Vip*- Male- $F(2,51) = 4.6$, $p < 0.05$, Female- $F(2,61) = 3.4$, $p < 0.05$; *Grp*- Male- $F(2,51) = 12.4$, $p < 0.005$, Female- $F(2,61) = 1.6$, $p = 0.2$). C-E, Daily transcript expression is double-plotted to facilitate visualization. Color-coded arrows indicate time of maximum expression in each sex. Scale bars = 100μm, ZT = Zeitgeber Time, a.u. = arbitrary units. $^{@}$Circwave test of rhythmicity, $p < 0.05$. * post hoc comparisons, $p < 0.05$.

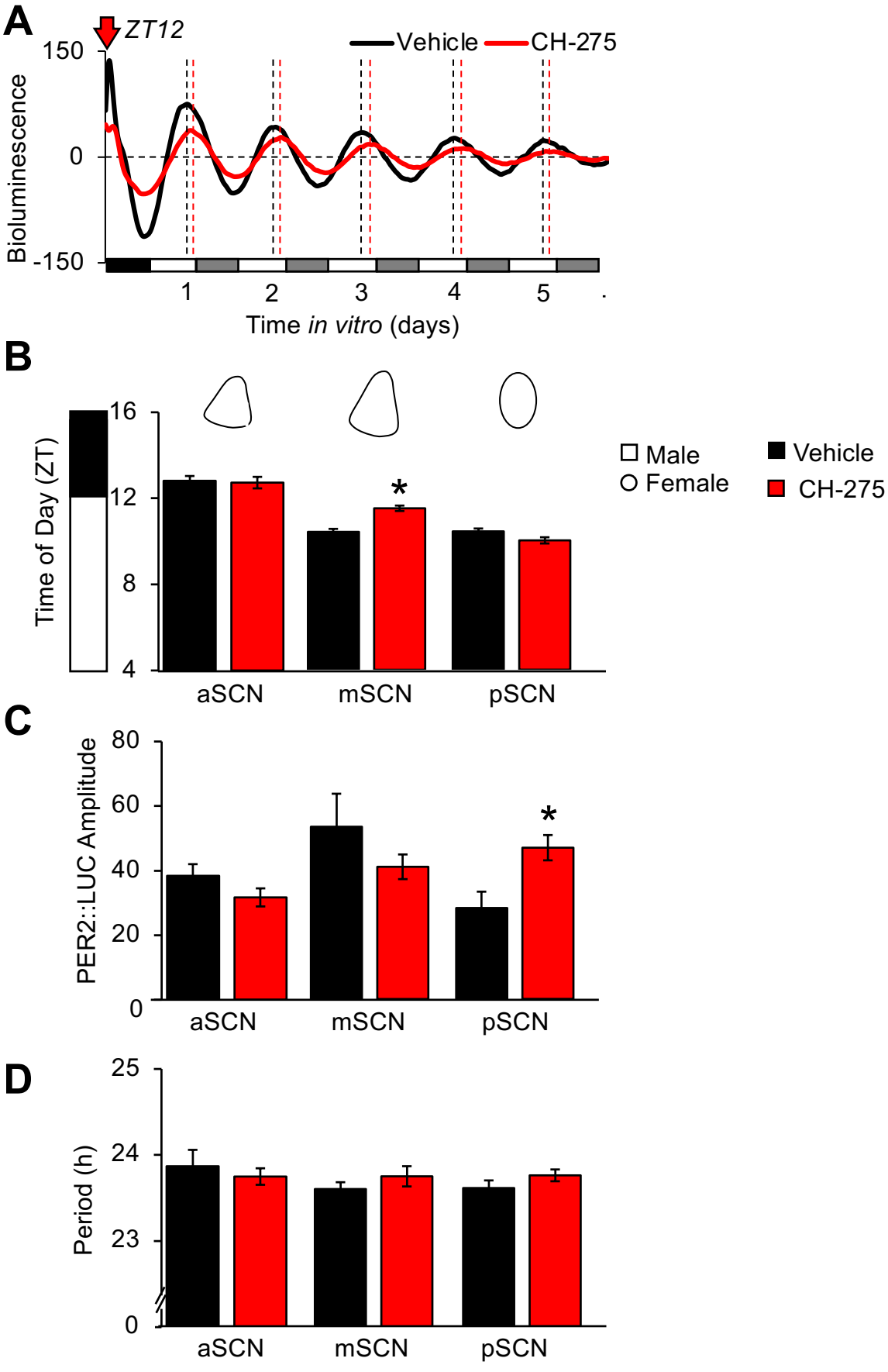
A
ZT12
Vehicle
CH-275
150
0
-150
Bioluminescence
1
2
3
4
5
Time in vitro (days)
B
16
12
8
4
Time of Day (ZT)
*
aSCN
mSCN
pSCN
Male
Female
Vehicle
CH-275
C
80
60
40
20
0
PER2::LUC Amplitude
*
aSCN
mSCN
pSCN
D
25
24
23
0
Period (h)
aSCN
mSCN
pSCN

FigureS9

Figure S9. SSTR1 agonists reset the SCN molecular clock. A) Representative time-series illustrating PER2::LUC rhythms after application of CH-275 (1μm) or vehicle at ZT12. B) ZT peak of PER2::LUC rhythms on Cycle1 *in vitro*. C) The SSTR1 agonist CH-275 modulated amplitude of PER2::LUC rhythms in the posterior SCN (pSCN- $F(1,14) = 7.3$, $p = 0.05$; aSCN- $F(3,15) = 1.3$, $p > 0.3$; mSCN- $F(3,16) = 1.3$, $p > 0.2$). D) CH-275 did not alter SCN period (aSCN- $F(3,15) = 0.2$, $p > 0.9$; mSCN- $F(3,16) = 0.8$, $p > 0.5$.; pSCN- $F(3,14) = 1.2$, $p > 0.3$). * post hoc comparisons, $p < 0.05$.

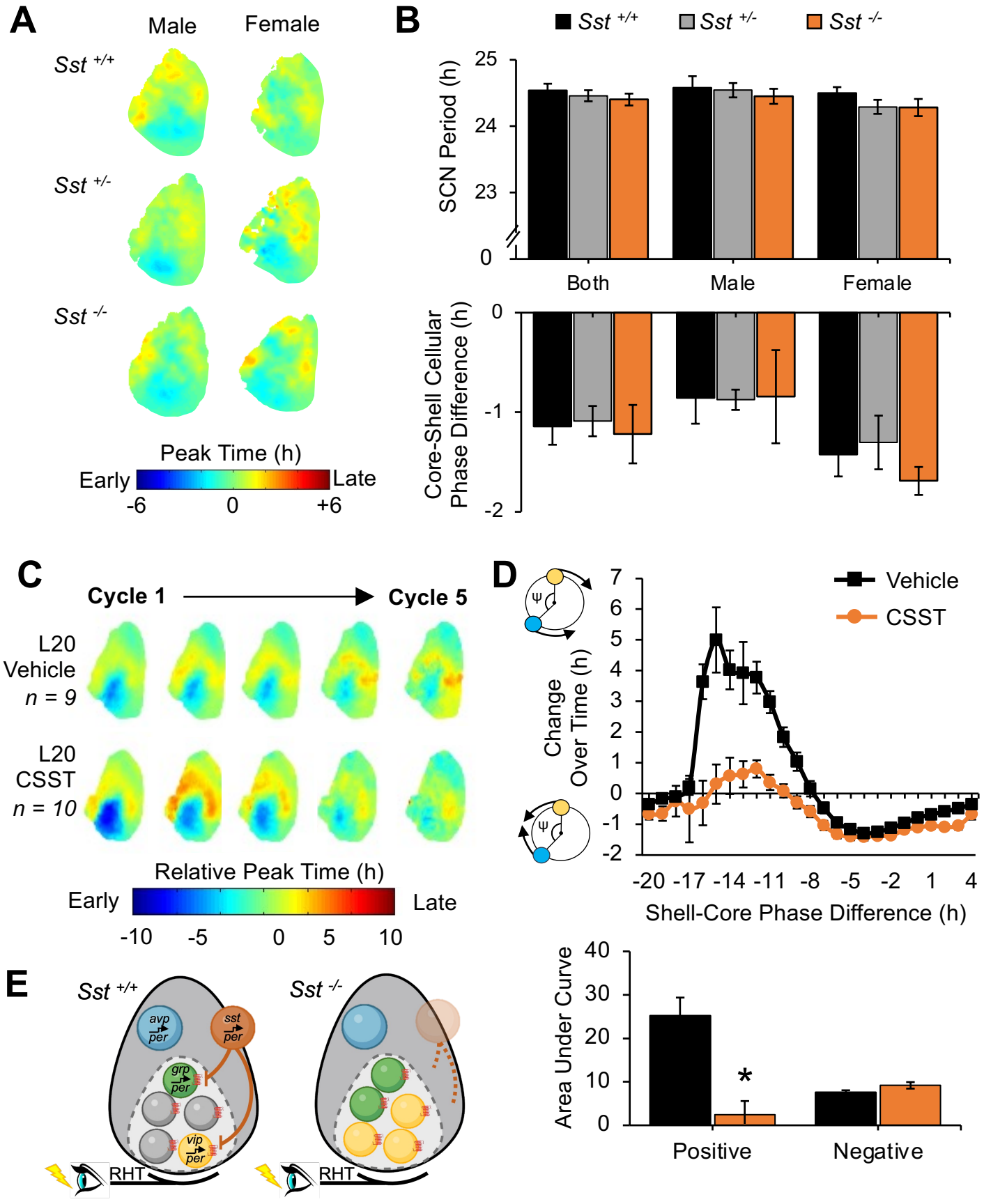
A
Male
Female
Sst +/+
Sst +/-
Sst -/-
Peak Time (h)
Early
Late
-6
0
+6
B
Sst +/+
Sst +/-
Sst -/-
SCN Period (h)
25
24
23
0
Both
Male
Female
Core-Shell Cellular Phase Difference (h)
0
-1
-2
C
Cycle 1
Cycle 5
L20 Vehicle n = 9
L20 CSST n = 10
Relative Peak Time (h)
Early
Late
-10
-5
0
5
10
D
Vehicle
CSST
Change Over Time (h)
7
6
5
4
3
2
1
0
-1
-2
-20 -17 -14 -11 -8 -5 -2 1 4
Shell-Core Phase Difference (h)
E
Sst +/+
Sst -/-
avp per
sst per
grp per
vip per
RHT
RHT
Area Under Curve
40
30
20
10
0
*
Positive
Negative

FigureS10

Figure S10. SST receptor antagonism reduces SCN coupling in adult wild-type male mice. A-B) Lack of SST did not alter SCN function under L12. SCN spatiotemporal organization ($F(5,35) = 1.9$, $p > 0.1$) and period ($F(5,35) = 1.3$, $p > 0.2$) did not differ by genotype, similar to the lack of behavioral effect prior to tissue collection (Alpha: $F(5,35) = 1.1$, $p > 0.3$). Male n = 7-8 mice/genotype, Female n = 4-8 mice/genotype. C) Composite phase maps of male SCN treated with vehicle (DMSO, < 0.1%) or the SST receptor antagonist cyclosomatostatin (CSST, 20μm). D) Top: Coupling response curves illustrating cellular resynchronization in male SCN treated with vehicle or CSST. Polar plots along Y-axis illustrate cellular dynamics (blue: SCN core neurons, yellow: SCN shell neuron, ψ: phase difference angle). Bottom: Area under the curve for positive and negative regions of the coupling response curve with and without CSST. (+AUC: $t(12) = 13.5$, $p < 0.001$; -AUC: $t(12) = 6.3$, $p < 0.001$). E) Schematic of working model, in which light activates SST-mediated modulation of SCN function, in part by inhibiting VIP/GRP expression (left), with disinhibition after loss of *Sst* (right) * post hoc comparisons, $p < 0.05$.